Journal of Sound and Vibration (2002) **252**(2), 317–341
doi:10.1006/jsvi.2001.4042 available online at http://www.idealibrary.com on IDEAL®

A GROUP THEORETIC APPROACH TO THE LINEAR FREE VIBRATION ANALYSIS OF SHELLS WITH DIHEDRAL SYMMETRY

S. J. Mohan and R. Pratap

Department of Mechanical Engineering, Indian Institute of Science, Bangalore 560 012, India

(*Received* 4 *May* 2001, *and in final form 12 September 2001*)

This paper deals with a group theoretic approach to the finite element analysis of linear free vibrations of shells with dihedral symmetry. Examples of such shell structures are cylindrical shells, conical shells, shells with circumferential stiffeners, corrugated shells, spherical shells, etc. The group theoretic approach is used to exploit the inherent symmetry in the problem. For vibration analysis, the group theoretic results give the correct symmetry-adapted basis for the displacement field. The stiffness matrix **K** and the mass matrix **M** are identically block diagonalized in this basis. The generalized linear eigenvalue problem of free vibration gets split into independent subproblems due to this block diagonalization. The Simo element is used in the finite element formulation of the shell equilibrium equations. Numerical results for natural frequencies and natural modes of vibration of several dihedral shell structures are presented. The results are shown to be in very good agreement with those reported in the literature. The computational advantages and physical insights due to the group theoretic approach are also discussed.

1. INTRODUCTION AND OVERVIEW

The problem of determining the values of natural frequencies and the corresponding mode shapes of structures is of much importance to engineers. The linear free vibration analysis is required for the determination of steady state response, the determination of transient response to forced vibration and is a prerequisite for the non-linear free vibration analysis. On the amplitude–frequency graph, the non-linear resonance backbone curves branch off at the linear natural frequencies.

In this paper, we deal with the group theoretic approach to the finite element analysis of linear free vibrations of shell structures with dihedral symmetry (i.e., the symmetry of a regular polygon). Many shells structures, analyzed separately in the literature, fall into this class. Examples of reported literature are results on cylindrical and conical shells extensively reviewed by Leissa [1] and Soedel [2], spherical shells with and without cutouts discussed in Niordson [3], shells with circumferential stiffeners reviewed by Soedel [2], etc. The common feature in all these shells is the dihedral symmetry and this is optimally exploited by the group theoretic approach.

The finite element analysis enables the implementation of general shell theories and thus an analysis of all kinds of shell structures with different boundary conditions (not always tractable by analytical methods). However, convergence requirements force the discretization to be so fine that the problem size usually ends up being huge ($\sim 20\,000 \times 20\,000$). The group theoretic approach enables an efficient solution procedure

0022-460X/02/$35.00

for these large-size problems. In particular, shells with complex geometry but with dihedral symmetry are amenable to efficient analysis due to group theory (see the last example in section 4). This approach achieves even greater prominence in non-linear analysis of shells (see references [4, 5]), where FEM analysis is indispensable. The analysis carried out in this work is the first step in the general (geometrically) non-linear vibration analysis of shells (to be reported in a future work).

Finding the natural frequencies of vibration of a shell using finite element discretization reduces to the generalized linear eigenvalue problem (see reference [6])

$$\mathbf{K}\Phi = \omega^2\mathbf{M}\Phi, \tag{1}$$

where $\mathbf{M}$ is the $n \times n$, symmetric, positive-semi-definite mass matrix, $\mathbf{K}$ is the $n \times n$, symmetric stiffness matrix, ω is one of the natural frequencies and Φ the corresponding mode shape. To exploit the symmetry of the shell, group representation theory can be used to construct an $n \times n$ orthogonal matrix $\mathbf{T}$ such that

$$\bar{\mathbf{K}} = \mathbf{T}^{\mathrm{t}}\mathbf{K}\mathbf{T} \quad \text{and} \quad \bar{\mathbf{M}} = \mathbf{T}^{\mathrm{t}}\mathbf{M}\mathbf{T} \tag{2}$$

each have the same block diagonal form. Thus, the original eigenvalue problem is split into independent subproblems. The analysis of free vibration of symmetric dihedral trusses is discussed by Healey and Treacy [6]. Healey [7] and Wohlever and Healey [4] used a group theoretic approach for non-linear bifurcation analysis of symmetric trusses and shells of revolution under static loads. Essentially, the group theoretic approach leads to the correct choice of the symmetry-adapted basis for the displacement vector field. The algorithm to construct this basis for dihedral truss structures is given by Ikeda and Murota [8]. This algorithm has been suitably modified and implemented for analysis of shells with dihedral symmetry by Wohlever [5]. We discuss the main ideas in section 3 and refer the reader to Wohlever [5] for detailed implementation notes.

The Simo element has been used in the finite element formulation of the shell equilibrium equations. This is a numerical implementation of the classical Cosserat shell theory. The implementation notes for this element are given in the papers by Simo *et al.* [9–12]. In the Simo element, a point on the shell is located by the position vector of its midsurface and a unit director vector along the material line (fibre). As opposed to most FE shell models, which have five degrees of freedom (three displacements of the midsurface and two rotations of the director), the Simo element has six degrees of freedom (d.o.f.) for each node. This is the result of considering the director displacement as an independent vector field. The director is thus extensible. Simo *et al.* [10] have used a mixed-variational formulation to avoid the problems of *membrane-locking* and *shear-locking*. The mixed-variational approach avoids the need to invoke procedures such as uniform or reduced integration. Thus, the full 2×2 Gauss integration is used and the element does not suffer from the problem of spurious modes. The weak form of the equilibrium equations are linearized exactly in the Simo element formulation. It is possible to work out a closed-form expression of the discrete tangent operator. This is important in the context of non-linear analysis, i.e., in the determination of the non-linear resonance curve which we will discuss in a future work. Overall, the performance of the Simo element compares well with the other state-of-the-art non-linear shell elements.

An outline of the remaining part of this paper is as follows. In section 2, we give a short description of the finite element formulation using the Simo element. In section 3, we discuss the relevant techniques of the group theoretic approach. In section 4, we present the numerical results of the free vibration analysis of several dihedral shell structures. These are shown to be in good agreement with the results reported in the literature. In section 5, we discuss the computational cost analysis of the group theoretic approach with

the help of CPU timings and floating point operations (flops) recorded during the numerical simulations. In section 6, we conclude with a discussion on the computational advantages and the physical insights due to the group theoretic approach.

The main goals of this work are: (1) to show that it is possible to carry out a free vibration analysis of a large class of engineering shell structures efficiently and accurately by a finite element analysis supplemented by group theoretic transformation routines; (2) to show the computational advantages and parallel processing options due to a group theoretic approach; and (3) to point out the physical insights provided by the role of symmetry in understanding the linear free response of thin shell structures.

2. THE SIMO SHELL ELEMENT

The classical Cosserat non-linear shell theory has been discussed by many authors. The important works are by Ericksen and Truesdell [13], Green and Laws [14], Green and Zerna [15], Cohen and DeSilva [16], and Naghdi [17] since the original work of Cosserat and Cosserat [18] in 1909. However, non-linear computational shell analysis has largely been carried out by the so-called "degenerated solid" approach originally proposed by Ahmed *et al.* [19]. This approach avoids the mathematical complexities associated with classical shell theory. In a series of papers, Simo *et al.* [9–12], demonstrated that classical shell theory that considers a shell as a single extensible director Cosserat surface lends itself to an efficient numerical implementation which is free from mathematical complexities and suitable for large-scale linear as well as non-linear computations.

We have used the Simo element for the finite element analysis of the shell equilibrium equations. We discuss briefly the special features of the Simo shell element in this section and refer the reader to the papers of Simo *et al.* [9–12] for details and implementation notes.

The kinematic description of the shell for the Simo element is as follows. A material point on the shell is parametrized by a co-ordinate system $(\xi_1, \xi_2, \eta) \in \mathscr{A} \times \mathscr{I}$, where $\eta \in \mathscr{I} = [h^-, h^+]$ is the "through the thickness parameter" and $\mathscr{A}$ and $\mathscr{I}$ are fixed regions in $\mathbf{R}^2$ and $\mathbf{R}$ respectively. The undeformed configuration $\mathscr{S} \subset \mathbf{R}^3$ of the shell in Euclidean space is a mapping $\Phi_0 : \mathscr{A} \times \mathscr{I} \to \mathbf{R}^3$,

$$\mathscr{S} := \{\mathbf{x}_0 \in \mathbf{R}^3 \mid \mathbf{x}_0 = \Phi_0(\xi_1, \xi_2, \eta) \ \forall (\xi_1, \xi_2, \eta) \in \mathscr{A} \times \mathscr{I}\}. \tag{3}$$

As shown in Figure 1, the material point $\mathbf{x}$ in any deformed configuration consistent with the single director assumption is given by

$$\mathbf{x} = \Phi(\xi_1, \xi_2, \eta) := \varphi(\xi_1, \xi_2) + \eta\, \mathbf{d}(\xi_1, \xi_2). \tag{4}$$

Here, $\varphi : \mathscr{A} \to \mathbf{R}^3$ defines the midsurface in $\mathscr{S}$, and $\mathbf{d} : \mathscr{A} \to \mathbf{R}^3$ defines the director field (or the thickness fibre). Thus, any deformed configuration $\mathscr{C}$ associated with the kinematic assumption is given by

$$\mathscr{C} := \{\Phi = (\varphi, \mathbf{d}) : \mathscr{A} \to \mathbf{R}^3 \times \mathbf{R}^3 \mid \mathbf{d} \cdot [\varphi_{,1} \times \varphi_{,2} 0\}. \tag{5}$$

Here, $\varphi_{,\alpha}$ denotes partial differentiation of φ with respect to ξ_α, $\alpha \in \{1, 2\}$. Any point in the shell configuration is defined by its position φ on the midsurface and a distance η along the director $\mathbf{d}$. The condition $\mathbf{d} \cdot [\varphi_{,1} \times \varphi_{,2}] > 0$ is required to prevent the possibility of infinite transverse shear.

The details regarding the derivation of local balance laws, the weak form of the equilibrium equations, the effective strain measures and the finite element implementation notes of the solution procedure considered in the formulation are discussed by Simo *et al.* [9–12]. The strain measures include terms that account for membrane, bending, transverse

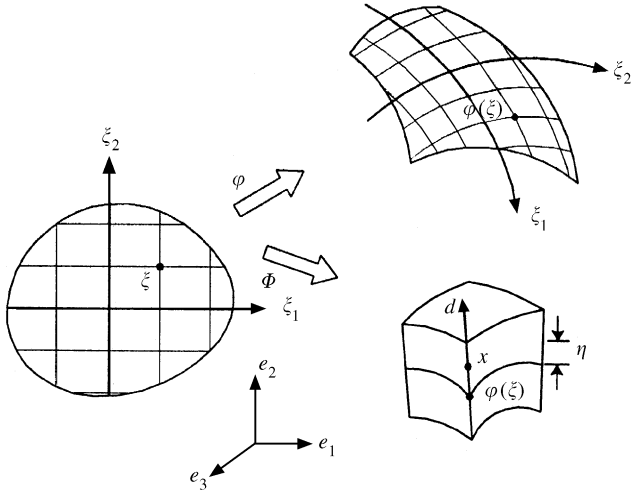

Figure 1. The kinematic assumption of the extensible director Cosserat surface.

shear, symmetric shear and the thickness stretch. In fact (see reference [12]), it can be shown that these strain measures give those components of the Lagrangian strain tensor from the three-dimensional theory, $\mathbf{E}$,[†] which are either independent or linear in η which is the through-the-thickness parameter.

Simo *et al.* [11] have also described a simple linear elastic isotropic constitutive model derived as per the standard procedures discussed by Green *et al.* [20]. The constitutive relations are enforced through a mixed variational approach which employs a Hellinger–Reissner functional (see reference [21]) for the membrane and thickness stretch fields and a Hu–Washizu functional (see reference [22]) for the transverse shear fields. The combined formulation effectively deals with the problems of *membrane-locking* and *shear-locking* and prevents the occurrence of spurious energy modes.

The expressions for the material stiffness matrix ($\mathbf{K}_{\mathrm{M}}$) and the geometric stiffness matrix ($\mathbf{K}_{\mathrm{G}}$) are given by Simo and Fox [12]. In this work, we deal with *linear* free vibrations only and hence require only the material stiffness matrix evaluated at the reference configuration, i.e., when all displacements are zero. The geometric stiffness matrix will be required if one wishes to compute the non-linear free vibration resonance curve.

The expression for the consistent mass matrix for the linear problem is given by the expression

$$\mathbf{M} = \int_{\bar{\mathscr{A}}} \bar{\rho}_0 N^A N^B \bar{j}_0 \, \mathrm{d}\xi_1 \, \mathrm{d}\xi_2 + \int_{\bar{\mathscr{A}}} \bar{I}_{0p} N^A N^B \bar{j}_0 \, \mathrm{d}\xi_1 \, \mathrm{d}\xi_2. \tag{6}$$

Here, N^A and N^B are standard isoparametric shape functions. As discussed in Simo *et al.* [23], typical approximations for the reference inertia terms are $\bar{\rho}_0 = 2h\rho_0$ and $\bar{I}_{0p} = (8h^3/12)\rho_0$, where ρ_0 is the reference mass density and $\bar{j}_0$ is the midsurface Jacobian in the reference configuration. In this approximation, the dependence of the three-dimensional density on the through-the-thickness variable, η, is neglected. The second term in equation (6) accounts for rotational inertia.

[†] $\mathbf{E} = 1/2(\mathbf{F}^{\mathrm{t}}\mathbf{F} - I)$, where $\mathbf{F}$ is the deformation gradient.

3. THE GROUP THEORETIC APPROACH

The basic results of group theory that are used to obtain the result in equation (2) are summarized in Appendix A. Group representation theory provides algorithms to compute the orthogonal transformation matrix **T**. The algorithms for trusses with dihedral symmetry are given by Ikeda and Murota [8]. These are easily adapted to the Simo element. The only significant difference for the Simo shell element is that the symmetry transformation must be applied twice per node, once for the displacement DOF of the midsurface and once for the displacement DOF of the director as discussed by Wohlever [5]. As mentioned earlier, the reader can refer to Wohlever [5] for detailed implementation notes for obtaining the symmetry transformation matrices.

3.1. THE FINITE ELEMENT MESH

A typical element and a finite element mesh for a shell of revolution are shown in Figure 2. The local node numbers 1–4 are used to locate the midsurface of the shell and nodes 5–8 are used to locate the outer surface of the shell. Each node has three d.o.f. Although this is an unusual way of defining a shell element, it is a convenient way to define both the thickness of the shell and the initial orientations of the directors at the nodes. The implementation of the Simo element appears three dimensional but the underlying equations are strictly two dimensional. The details of the reduction of the three-dimensional equilibrium equations to equilibrium equations on the midsurface via integration through the thickness are given by Simo and Fox [9].

The FE mesh must be symmetric to obtain shell equilibrium equations with the required symmetry. A mesh with the symmetry of the dihedral group, D_n, is achieved by m uniform *rings* of n elements about the circumference with each element subtending an angle of $2\pi/n$ radians at the centre. Thus, a typical mesh for a shell with dihedral symmetry consists of n elements around the circumference and $m-1$ elements down its length. For such a mesh, the largest symmetry group which could be realized in the discrete FE equations would be the dihedral group D_n. Consider the kth ring of this mesh ($k = 1, 2, \ldots, m$). The configuration space for a given ring (V^{k}_{ring}) is a $3 \times 2n = 6n$-dimensional vector space. Therefore, the dimension of the complete displacement vector space is $6mn$. The stiffness matrix **K** and mass matrix **M** are assembled using a fixed XYZ cartesian coordinate system for the displacements. Thus the matrices **K** and **M** $\in \mathbf{R}^{6mn \times 6mn}$. The structures of a typical stiffness and the corresponding mass matrix are shown in Figure 3.

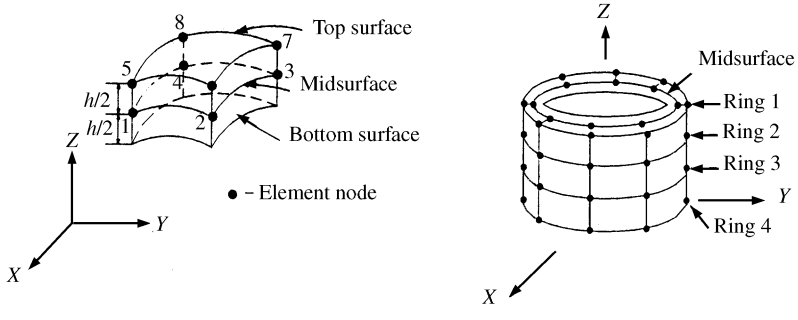

Figure 2. The Simo element and a typical FEM dicretization of a shell.

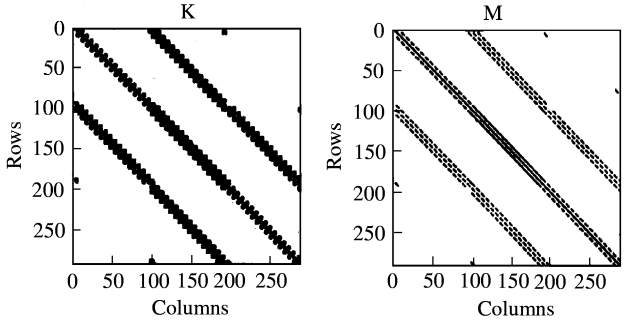

Figure 3. Location of the non-zero entries in the assembled stiffness matrix **K** and the consistent mass matrix **M** in the standard basis.

3.2. THE STRUCTURE OF THE LINEAR TRANSFORMATION T

The similarity transformation by **T** (as per equation (2)) changes the basis of the displacement vector field V into one in which the stiffness matrix **K** and mass matrix **M** are block diagonalized. There are N mutually orthogonal subspaces V_j, $j = \{1, 2, \ldots, N\}$, where N is the number of inequivalent irreducible representations of the symmetry group G. Thus, $V_j \equiv span\{e_i^j\}(i = 1, 2, \ldots, c_j)$, where $\{e_i^j\}$ is an orthonormal set of basis vectors for the subspace V_j, such that

$$V = V_1 \oplus V_2 \oplus \cdots \oplus V_N. \tag{7}$$

This isotypic decomposition of the vector space V is unique. The dimensions of the subspaces $c_j = |V_j|$ are also uniquely determined. It can be shown (see reference [8]) that each one of the subspaces, V_j, reflects part of the symmetry of the original system. This result leads to physical insights which are unique to the group theoretic approach. The subspace V_1 is typically designated as the G-invariant subspace which implies that the elements of V_1 reflect the symmetry of the complete group G. For example, V_1 might represent the set of all axisymmetric solutions in a problem with circular symmetry. The symmetry of the subspace V_j can be determined by the associated *isotropy subgroup*.

We recall that for a mesh with the symmetry of the dihedral group, D_n, and m rings along the length, the vector space of displacements is of dimension $6mn$. The structure of the orthogonal linear transformation **T** will thus be of the form

$$\mathbf{T} = [\mathbf{T}_1\ \mathbf{T}_2\ \mathbf{T}_3\ \ldots\ \mathbf{T}_N] \in \mathbf{R}^{6mn \times 6mn}, \tag{8}$$

where $\mathbf{T}_j = [e_1^j, e_2^j, \ldots, e_{c_j}^j]$, are $(6mn \times c_j)$ matrices whose columns are made up of the orthonormal symmetry-adapted basis vectors for V_j. In particular, the orthogonal matrix $\mathbf{T} \in \mathbf{R}^{6mn \times 6mn}$ depends on whether n is even or odd. If n is even, **T** is of the form

$$\mathbf{T} = [\mathbf{T}_1\ \mathbf{T}_2\ \mathbf{T}_3\ \mathbf{T}_4\ \mathbf{T}_{(1,1)}\ \mathbf{T}_{(1,2)}\ \ldots\ \mathbf{T}_{(2,1)}\ \mathbf{T}_{(2,2)}\ \ldots\ \mathbf{T}_{(2,p)}], \quad p = \frac{n-2}{2}. \tag{9}$$

If n is odd, then

$$\mathbf{T} = [\mathbf{T}_1\ \mathbf{T}_2\ \mathbf{T}_{(1,1)}\ \mathbf{T}_{(1,2)}\ \ldots\ \mathbf{T}_{(2,1)}\ \mathbf{T}_{(2,2)}\ \ldots\ \mathbf{T}_{(2,p)}], \quad p = \frac{n-1}{2}, \tag{10}$$

where $\mathbf{T}_1$–$\mathbf{T}_4$ in equation (9) and $\mathbf{T}_1$–$\mathbf{T}_2$ in equation (10) are associated with the four *one-dimensional* irreducible representations and $\mathbf{T}_{(1,1)}$–$\mathbf{T}_{(2,p)}$ with the *two-dimensional* irreducible representations. Moreover, $\mathbf{T}_{(1,k)} \equiv \mathbf{T}_{(2,k)}$, $k = 1, 2, \ldots, p$, i.e., they are equivalent matrices in terms of their eigenspectrum. The symmetry of the subspaces V_j is given by

isotropy subgroups $g(.)$ associated with the columns of $\mathbf{T}_j$. These are

$$g(\mathbf{T}_1) = D_n, \qquad g(\mathbf{T}_2) = C_n, \qquad g(\mathbf{T}_3) = g(\mathbf{T}_4) = D_{n/2}, \tag{11}$$

$$g(\mathbf{T}_{(\alpha,j)}) = D_{gcd(n,j)}, \qquad (\alpha = 1,2), \quad j = \begin{cases} 1,\ldots,\frac{n-1}{2} & \text{(odd } n\text{)}, \\ 1,\ldots,\frac{n-2}{2} & \text{(even } n\text{)}. \end{cases} \tag{12}$$

The operator $gcd(i,j)$ is the greatest common divisor of i and j. For a more detailed discussion on the structure of $\mathbf{T}$, the reader is referred to Ikeda and Murota [8].

3.3. SIGNIFICANCE OF THE BLOCK DIAGONALIZATION

The non-zero entries of the stiffness matrix $\mathbf{K}$ and the mass matrix $\mathbf{M}$ (shown in the standard basis in Figure 3) are shown in Figure 4 in the symmetry-adapted basis. It is clear from the block diagonalization that,

(1) The original generalized linear eigenvalue problem is split up into lower dimensional independent subproblems. For example, the blocks of the stiffness and mass matrices ($\tilde{\mathbf{M}}$ and $\tilde{\mathbf{K}}$) in the symmetry-adapted basis are shown in Figure 4. These are seven independent subproblems of the original generalized eigenvalue problem.
(2) One can determine *a priori* the size of the lower dimensional matrices. The explicit formulae for the dimensions of the subproblems are discussed by Ikeda and Murota [8]. Consider a D_N symmetric FE mesh with n circumferential elements and m rings along the length. The original problem size has $6mn$ d.o.f. As discussed by Wohlever [5], if (n/N) and N are even, then the sizes of the four subproblems associated with the one-dimensional irreducible representations are $m(3n/N + 2)$, $m(3n/N - 2)$, $(3mn/N)$ and $(3mn/N)$, respectively, and the dimension of the p subproblems associated with the two-dimensional representations is $6mn/N$ (see section 4 for examples).
(3) One can determine *a priori* the number of subproblems which are identical in terms of their eigenspectrum. Thus, equations (9) and (10) imply that there are p pairs of equivalent subproblems in the block diagonalization. Thus, only the first p subproblems need to be analyzed for a complete eigenanalysis of the original problem (see section 4 for examples).

Moreover, each block reflects part of the symmetry of the original system. Thus, each of the blocks in the block diagonalized stiffness matrix $\tilde{\mathbf{K}}$ and mass matrix $\tilde{\mathbf{M}}$ (equations (11)

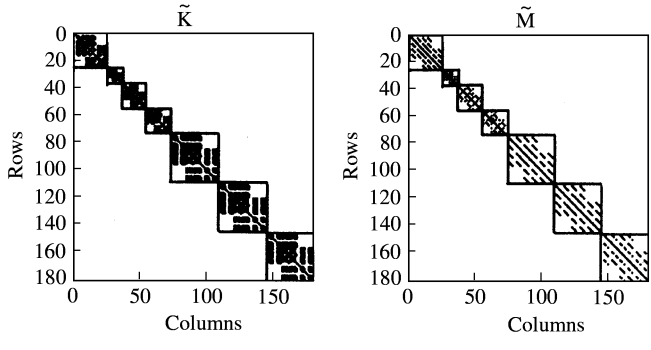

Figure 4. Location of the non-zero entries of the assembled stiffness matrix $\tilde{\mathbf{K}}$ and the consistent mass matrix $\tilde{\mathbf{M}}$ in the symmetry-adapted basis.

and (12)) group together all the vibration modes which possess the symmetry of the associated *isotropy subgroup*.

3.4. PSEUDO CODE

The algorithm used for the determination of the natural frequencies and the corresponding mode shapes is given below. An important computational note is that most of the work is done in the standard computational basis. The symmetry co-ordinates are used only in the eigenvalue analysis. Thus, the group theoretic transformation routines can be appended to any existing FE code to aid in the analysis of symmetric problems.

- *Compute* the stiffness matrix $\mathbf{K}$ and the mass matrix $\mathbf{M}$ in the standard basis.
- *Compute* the transformation matrix $\mathbf{T}_j$.
- *Transform* $\tilde{\mathbf{K}}_j = \mathbf{T}_j^{\mathrm{t}}\mathbf{K}\mathbf{T}_j$, $\tilde{\mathbf{M}}_j = \mathbf{T}_j^{\mathrm{t}}\mathbf{M}\mathbf{T}_j$.
- *Solve* $\tilde{\mathbf{K}}_j\tilde{\boldsymbol{\Phi}}_j = \omega_j^2\tilde{\mathbf{M}}_j\tilde{\boldsymbol{\Phi}}_j$ in symmetry co-ordinates.
- *Transform* $\boldsymbol{\Phi}_j = \mathbf{T}_j\tilde{\boldsymbol{\Phi}}_j$ into standard basis for post-processing.

4. RESULTS AND DISCUSSION

In this section, we present the numerical results of the FEM analysis for several shell structures. The results compare well with the analytical and experimental values reported in the literature. The analytical results for simple shell structures depend on an "inspired guess" of the mode shapes. However, this would be impossible for a complicated assembly of basic shell structures. The group theoretic approach offers a systematic procedure to choose an optimal symmetry-adapted basis, as long as it is ensured that the dihedral symmetry of the problem is imposed on the FE mesh. We illustrate this through the analysis of a combination structure, a typical pressure vessel, presented as the final example.

4.1. CYLINDRICAL SHELLS

The results of the FEM analysis on a thin cylindrical shell are presented in Table 1. The stiffness matrix $\mathbf{K}$ and mass matrix $\mathbf{M}$ are block diagonalized with the representation of the group D_{24}. Although there are 48 elements along the circumference which should ideally be analyzed with the D_{48} group representation, we have presented the analysis of a reduced group representation D_{24} so that we can present the analysis of all the subproblems in the block diagonalization. Thus there are 27 subproblems with a D_{48} representation whereas the D_{24} representation has 15 subproblems as per equation (9), the first four associated with the *one-dimensional* irreducible representations and the next 11 associated with the *two-dimensional* irreducible representations (see Appendix A). The first two eigenvalues of each block are calculated using the Lanczos routine. The mode shapes associated with these natural frequencies are plotted in Figures 5 and 6. These results are compared with the analytical solution reported by Soedel [2] in Figure 7(a). We also carried out the same analysis with the D_{48} group representation and found no difference in the values of the eigenvalues (natural frequencies). The natural frequencies are in good agreement with the analytical solution upto 5–6 circumferential waves. There are only 48 elements along the circumference in the FEM mesh. The accuracy at higher number of circumferential waves can be improved by finer discretization along the circumference. For example, we carried out the analysis with 144 elements along the circumference and a D_{144} group

TABLE 1

Free vibration analysis of cylindrical shells

Block no.	Block size	Isotropy subgroup	First natural frequency 1/2 axial wave	Second natural frequency 1 axial wave	No. of circumferential waves
1	88×88	D_{24}	49 870	51 078	0
2	44×44	C_{24}	50 000	101 232	0
3	66×66	D_{12}	63 889	65 857	6
4	66×66	D_{12}	63 889	65 857	6
5	132×132	D_1	30 866	45 767	1
6	132×132	D_2	17 802	35 912	2
7	132×132	D_3	11 028	27 296	3
8	132×132	D_4	8658	21 441	4
9	132×132	D_1	9625	18 607	5
10	132×132	D_6	12 780	18 771	6
11	132×132	D_1	17 395	21 572	7
12	132×132	D_8	23 308	26 505	8
13	132×132	D_3	30 624	33 289	9
14	132×132	D_2	39 580	41 930	10
15	132×132	D_1	50 516	52 652	11

Note: Geometrical data: radius $r = 100$ mm, thickness $h = 2$ mm, length $L = 200$ mm. Material properties: $E = 20{\cdot}6 \times 10^4$ N/mm^2, $\rho = 7{\cdot}85 \times 10^{-9}$ N s^2/mm^4, $\mu = 0{\cdot}3$. FEM data: no. of circumferential elements = 48, no. of longitudinal rings = 11, d.o.f = 3168, boundary condition: *simply supported*. Symmetry group representation: D_{24}.

representation and found very good agreement with the analytical result presented by Soedel [2] even for the mode shape with eight circumferential waves. The analytical value is 2×10^4 rad/s while the value obtained by our FEM analysis was $2{\cdot}07 \times 10^4$ rad/s. The comparison of the results of Soedel [2] at higher discretization of the FEM mesh (144 elements along the circumference) is also shown in Figure 7(b).

It is clear that the block diagonalization reflects the role of symmetry in the phenomenon of free vibrations of cylindrical shells. The lowest frequency in each block is associated with a 1/2 axial wave. The next value is associated with a unit axial wave and so on. The first block captures the axisymmetric solutions, the second block the torsional mode (i.e., the mode which preserves cyclic symmetry). The number of circumferential waves increases uniformly from the fifth block onwards (the blocks associated with the two-dimensional irreducible representations). The lower frequencies of vibrations are closely spaced together, as observed from the lowest values in blocks 7–10. Also, it is well known that the number of circumferential waves at the fundamental frequency of the shell is a function of the shell geometry. To quote Leissa [1], "There appears to be no simple rule for determining the spacing of the frequencies as the wave numbers are varied". In contrast to vibrations of beams and plates, the lowest frequencies increase as the number of axial waves is increased but decrease to a minimum before they increase as the number of circumferential waves is increased. An explanation for this anomalous behaviour is given by Kraus [24] and Arnold and Warburton [25] from a consideration of the strain energy associated with the bending and stretching of the reference surface. They demonstrated the relative contribution of the two forms of strain energy associated with the lowest natural frequency of the variational solution. At low circumferential wave numbers, the bending strain energy is low and stretching strain energy is high. At higher wave numbers it is just the reverse. This interchange in relative contribution to the total strain energy with increasing number of circumferential waves is responsible for the anomalous behaviour in the lowest frequency analysis. Thus, an analysis of the lower

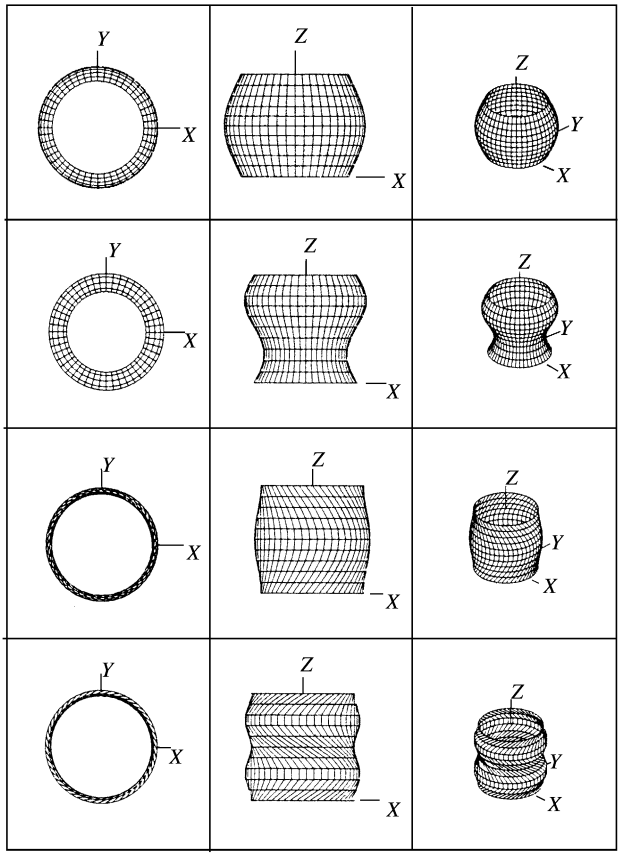

Figure 5. The mode shapes of the cylindrical shell associated with the lowest two natural frequencies of blocks 1 and 2. The first column shows the top view, the second column shows the corresponding front view and the third column shows an isometric view of each mode shape.

natural frequencies of the cylindrical shell will require the determination of the vibration modes with circumferential waves varying from 0 to 6 or 7. There is a neat separation of these closely spaced vibration modes in the block diagonalization, i.e., these frequencies fall into different blocks. Also, it is observed that there is a large difference in the value of the first two frequencies within each block. Thus, the numerical conditioning of the stiffness matrix has been considerably improved due to the group theoretic block diagonalization.

From the computational point of view, there is a considerable decrease in problem size. The size of the original stiffness matrix is 3168×3168 while the largest block size is only 132×132. Each block is an independent subproblem of the original generalized eigenvalue problem. Thus, apart from the huge reduction in the size of the problem that needs to be solved there is an option of parallel processing due to a group theoretic analysis.

4.2. SPHERICAL SHELLS

The literature on free vibrations of thin elastic spherical shells is vast. A review and extensive bibliography is given by Kraus [24] and Leissa [1]. In this section, we compare

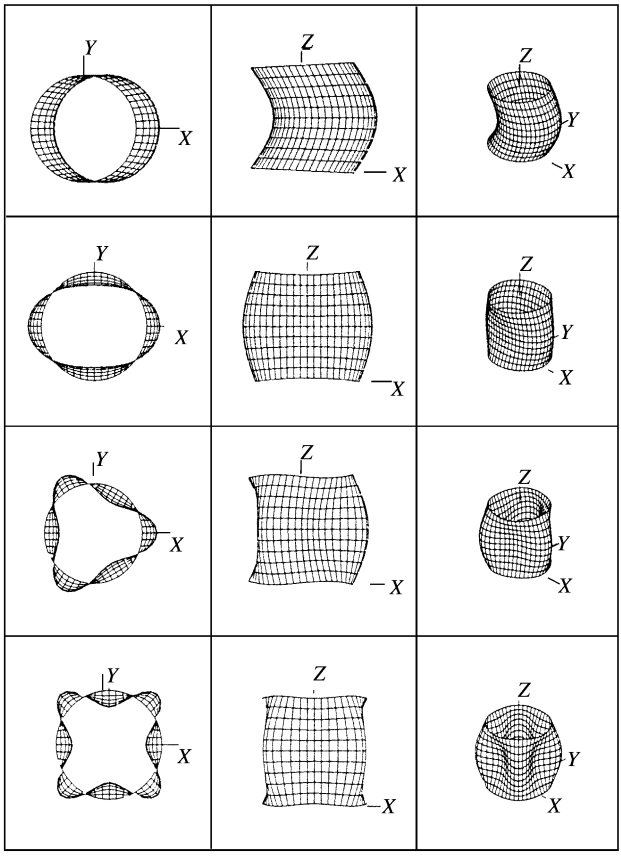

Figure 6. The mode shapes of the cylindrical shell associated with the lowest natural frequency of blocks 5–8. The first column shows the top view, the second column shows the corresponding front view and the third column shows an isometric view of each mode shape.

the results of the numerical simulations with the relatively recent analytical results of Niordson [3]. The author has given complete solutions for axisymmetric and non-axisymmetric vibrational modes for a shell in the shape of a spherical zone with two boundaries. The hemispherical shell with a circular cutout is a special case of this general solution.

The comparison of the FEM numerical simulation results with the analytical results is given in Table 2. There is excellent agreement between the two in all the cases. The corresponding mode shapes are shown in Figure 8. The following observations of Niordson [3] are clearly reflected in the mode shapes of the free vibrations. The bending of thin shells is confined to a comparatively narrow region at the boundary, the first lower natural frequency is strongly dependent on the size of the larger opening, and the second lower natural frequency is more or less determined by the smaller opening.

4.3. CONICAL SHELLS

The free vibration studies on conical shells have also been extensive. A complete chapter deals with conical shells in the review by Leissa [1, chapter 5]. The cylindrical shell is just a special case of the conical shell with zero conical angle. In an earlier paper, Grigolyuk [26]

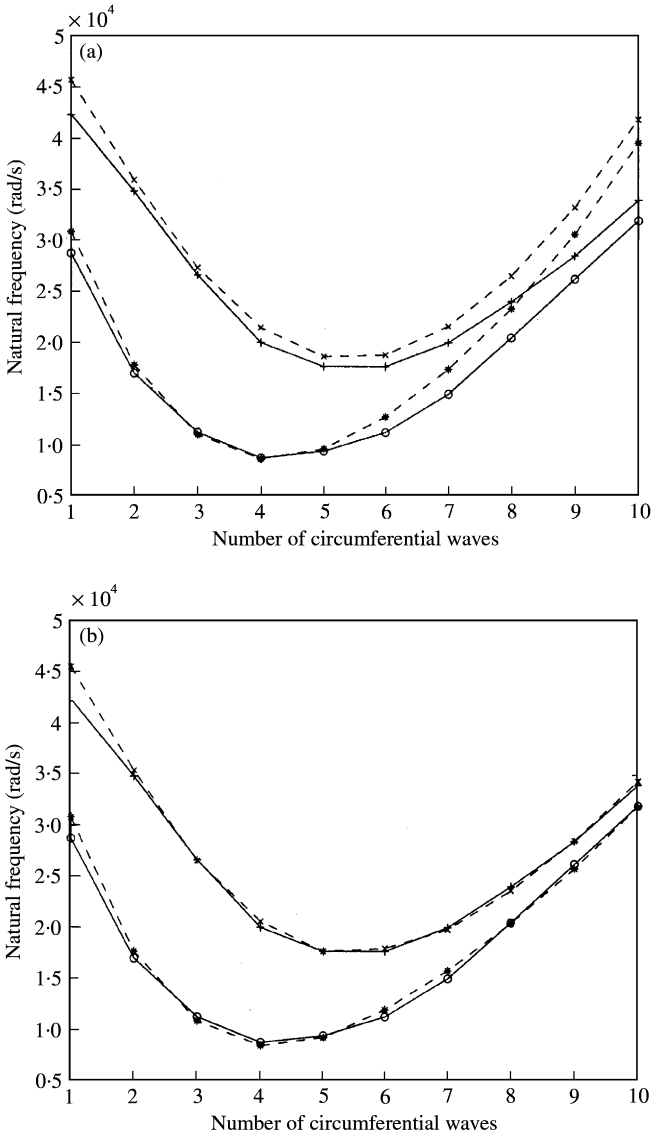

Figure 7. The comparison of the FEM numerical results with the results of Soedel [2]. (a) Results with coarse discretization (48 circumferential elements). Results from all blocks of the D_{24} representation are given in Table 1. (b) Results with finer discretization (144 circumferential elements). Note that the agreement with the results of Soedel [2] improves significantly at higher circumferential waves. ○——○, Analytical solution (first natural frequency); ∗---∗, FEM solution (first natural frequency); +——+, analytical solution (second natural frequency); ×---×, FEM solution (second natural frequency).

suggested that for purposes of calculations, shells having small conicity can be adequately represented by circular cylindrical shells with radius equal to the average conical shell radius. However, subsequent results of researchers have shown that this is not a good approximation (refer to the results of Platus [27]).

Just as for cylindrical shells, the fundamental frequency of a conical shell does not occur at $n = 0$ (i.e., it is not axisymmetric and has a few circumferential waves). We pick the case of a conical frustum with a clamped-free boundary condition for our numerical results. This has received much treatment in the literature because of its widespread use in

TABLE 2

Free vibration analysis of spherical shells

No. of Circumferential waves	First natural frequency coefficient "c" Niordson's soln.	First natural frequency coefficient "c" FEM solution	Second natural frequency coefficient "c" Niordson's soln.	Second natural frequency coefficient "c" FEM solution
2	2·0275	2·029	8·2272	8·248
3	5·7068	5·738	Not available	Not available
4	10·8128	10·96	Not available	Not available
5	17·1278	17·65	Not available	Not available

Note: Geometrical data: radius $r = 100$ mm, thickness $h = 1$ mm, cutout angle $\alpha = 30^\circ$. Material properties: $E = 20{\cdot}6 \times 10^4$ N/mm^2, $\rho = 7{\cdot}85 \times 10^{-9}$ N s^2/mm^4, $\mu = 0{\cdot}3$. FEM data: no. of circumferential elements= 48, no. of longitudinal rings= 19, $d.o.f. = 5472$, boundary condition: *free–free*. Non-dimensional coefficient $c = (\omega r^2/h) \times \sqrt{2\rho(1+\mu)/E}$.

practical design as loudspeaker cones. The comparison with the numerical and experimental results of Platus [27] is shown in Figure 9. The agreement is excellent. The corresponding mode shapes of the first four natural frequencies in the symmetry block with the lowest natural frequency are shown in Figure 10.

4.4. A COMBINATION STRUCTURE: PRESSURE VESSEL

While the literature is abound with analytical results which give accurate answers for common shell geometries, a typical engineering structure is usually an assembly of these basic shell structures. These analytical solutions generally depend on an inspired guess of the mode shapes. However, a structure as an assembly of basic shell structures will require an FEM analysis for accurate and reliable results. Here, we consider an assembly of a conical frustum, a cylindrical body and a hemispherical dished end with a cutout. This complicated assembly represents a typical pressure vessel. This geometry is efficiently dealt with by a group theoretic approach to the FEM analysis. We have already demonstrated the advantages and accuracy of such an approach in the previous three examples. The essential ingredient is dihedral symmetry, which is preserved in this assembly of the basic shell structures. Thus, the assembly does not add any further complexity to the problem as far as the group theoretic approach is concerned.

The results of the complete analysis for the clamped–clamped boundary conditions are presented in Table 3. The convergence of the values of the first two natural frequencies in a few blocks (blocks 8, 11 and 15, chosen arbitrarily) with finer FEM meshes is shown in Figure 11. Similar convergence results were obtained in all the other blocks though the results have not been presented here to avoid clutter in the figures. As with cylindrical shells, the lowest fundamental natural frequency decreases with an increase in the number of circumferential waves to a minimum before increasing again. In this example the fundamental frequency is in block 9, the block with D_5 symmetry, i.e., five circumferential, waves. The mode shapes of the block with the lowest frequency are shown in Figure 12. The lowest natural frequency is primarily dependent on the cylindrical structure and the next natural frequency on the conical structure. It is only in the fourth mode that all the three-component structures participate.

This problem requires heavy discretization for accurate calculation of the natural frequencies. Therefore, we take an FEM mesh with 144 elements along the circumference and 37 rings along the length of the structure. This mesh leads to a problem size of $31\,968 \times 31\,968$. However, the analysis by a D_{144} representation leads to a maximum

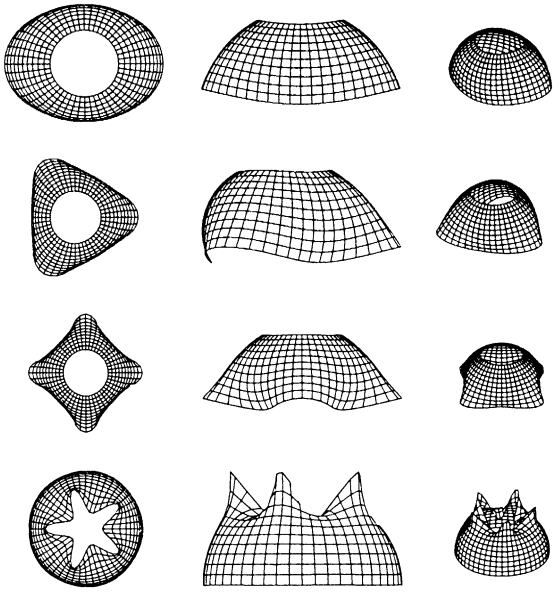

Figure 8. The mode shapes of the spherical shells associated with the lower natural frequencies of blocks 6–9. The first column shows the top view, the second column shows the corresponding front view and the third column shows an isometric view of each mode shape.

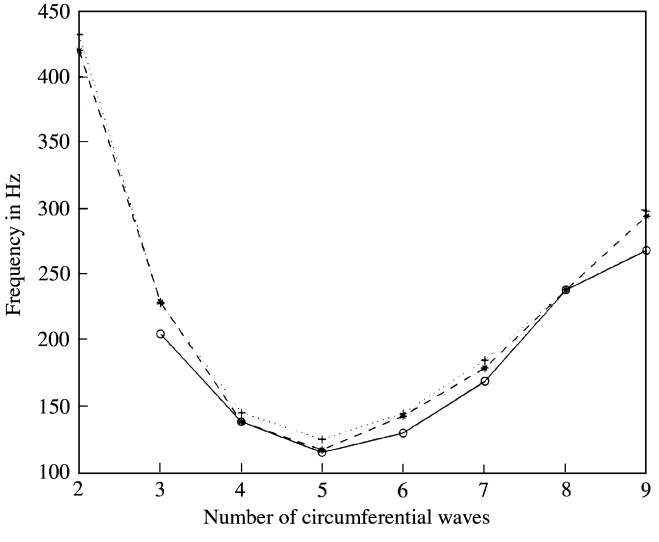

Figure 9. The comparison of FEM numerical results for a conical frustum with the experimental and analytical values reported by Platus. ○——○, Experimental values; ∗- - - ∗, analytical solution; + ⋯ +, FEM solution.

subproblem size of 222 × 222 as shown in Table 3 (this is a reduction in the problem size by a factor of ∼ 100). We note that though the number of independent subproblems are considerably more (71 as per equation (9)), only a few of these blocks have to be analyzed to obtain the lower natural frequencies and the corresponding mode shapes. The results of the analysis of the first 15 blocks are shown in Table 4. Blocks 1–4 are associated with *one-dimensional* group representations and the remaining blocks are associated with

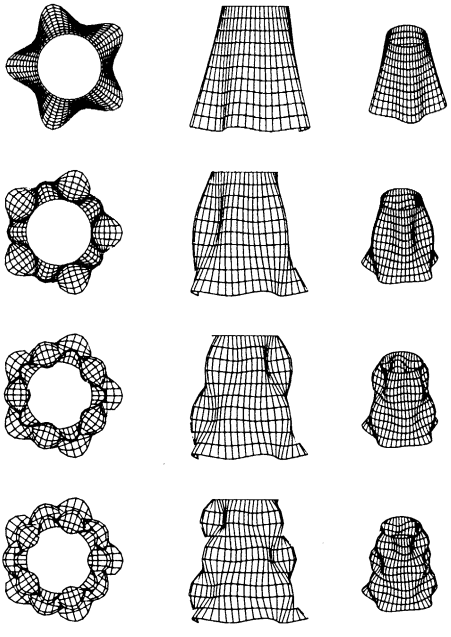

Figure 10. The mode shapes of a conical shell associated with the first four natural frequencies in block 9. The first column shows the top view, the second column shows the corresponding front view and the third column shows an isometric view of each mode shape.

TABLE 3

Free vibration analysis of a pressure vessel

Block no.	Block size	Isotropy subgroup	First natural frequency 1/2 axial wave	Second natural frequency 1 axial wave	No. of circumferential waves
1	148×148	D_{144}	21 797	43 931	0
2	74×74	C_{144}	22 725	62 994	0
3	148×148	D_{72}	496 860	526 892	6
4	74×74	D_{72}	503 348	520 671	6
5	222×222	D_1	22 214	34 219	1
6	222×222	D_2	20 270	33 860	2
7	222×222	D_3	17 328	28 274	3
8	222×222	D_4	14 924	25 839	4
9	222×222	D_1	14 176	26 512	5
10	222×222	D_6	15 426	29 678	6
11	222×222	D_1	18 358	31 309	7
12	222×222	D_8	22 520	33 641	8
13	222×222	D_3	27 635	37 380	9
14	222×222	D_2	33 566	42 327	10
15	222×222	D_1	40 256	48 320	11

Note: Cone dimensions: cone angle $\beta = 45^\circ$, thickness $h = 2$ mm, length $L = 50$ mm. Cylinder dimensions: radius $r = 100$ mm, thickness $h = 2$ mm, length $L = 200$ mm. Hemisphere dimensions: radius $r = 100$ mm, thickness $h = 1$ mm, cutout angle $\alpha = 30^\circ$. Material properties: $E = 20{\cdot}6 \times 10^4$ N/mm^2, $\rho = 7{\cdot}85 \times 10^{-9}$ N s^2/mm^4, $\mu = 0{\cdot}3$. FEM data: no. of circumferential elements= 144, no. of longitudinal rings= 37, *d.o.f.* = 31968, boundary condition: *clamped–clamped*. Symmetry group representation: D_{144}.

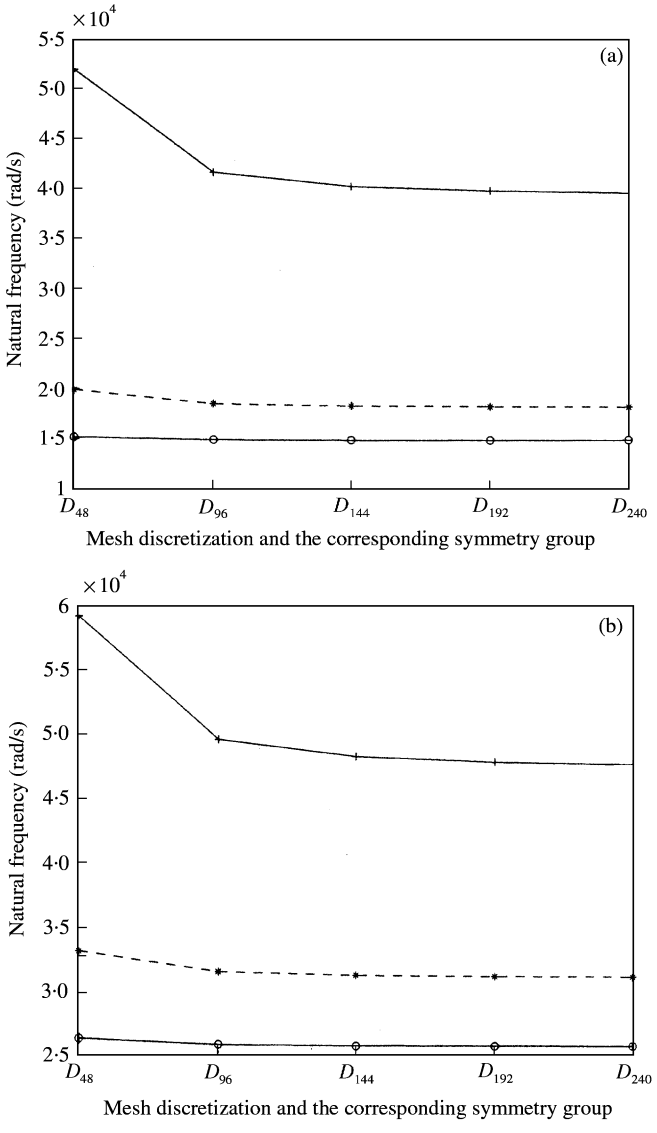

Figure 11. The convergence of the values of the natural frequencies with finer discretization of the FEM mesh in the free vibration analysis of the pressure vessel (a) shows the convergence of the values of the first natural frequency and figure (b) shows the convergence of the values of the second natural frequency. ○——○, Block 8 (4 circumferential waves); ∗- - -∗, Block 11 (7 circumferential waves); +——+, Block 15 (11 circumferential waves).

two-dimensional group representations. It is clear that block 1 is associated with the axisymmetric vibration mode shape (with low natural frequencies) and blocks 2–4 are associated non-axisymmetric mode shapes (with higher natural frequencies). After block 1, we need to look at only a few blocks from block 5 onwards because these blocks capture mode shapes with increasing number of circumferential waves.

5. COMPUTATIONAL COST ANALYSIS

The computational efficiency of the group theoretic approach can perhaps be measured by noting the *floating point operations* (flops) and the CPU time during actual program

TABLE 4

Computational savings in CPU time and flop count

D_n symmetry group	8	16	32	64	128
Size of $\mathbf{K}$ and $\mathbf{M}$ $N \times N$	528	1056	2112	4224	8448
Size of $\tilde{\mathbf{K}}_j$ and $\tilde{\mathbf{M}}_j$ $N_j \times N_j$	66	66	66	66	66
Eigenanalysis $\mathbf{Ku} = \omega^2\mathbf{Mu}$ Mega flops	44	120	680	1330	3800
Assembly of $\mathbf{T}$	0·08	0·22	0·34	0·86	1·75
Similarity transformation $\tilde{\mathbf{K}}_j = \mathbf{T}_j^t\mathbf{K}\mathbf{T}_j$ and $\tilde{\mathbf{M}}_j = \mathbf{T}_j^t\mathbf{M}\mathbf{T}_j$ Mega flops					
Block eigenanalysis $\tilde{\mathbf{K}}_j\mathbf{u} = \omega^2\tilde{\mathbf{M}}_j\mathbf{u}$ Mega flops	1·65	1·65	1·7	1·7	1·7
Normalized flops†	5·2	12·8	64·7	103·5	217·1
Eigenanalysis $\mathbf{Ku} = \omega^2\mathbf{Mu}$ CPU time (s)	16·8	41·8	194·2	399·3	1052
Assembly of $\mathbf{T}$	0·04	0·08	0·16	0·32	1·03
Similarity transformation $\tilde{\mathbf{K}}_j = \mathbf{T}_j^t\mathbf{K}\mathbf{T}_j$ and $\tilde{\mathbf{M}}_j = \mathbf{T}_j^t\mathbf{M}\mathbf{T}_j$ CPU time (s)					
Block eigenanalysis $\tilde{\mathbf{K}}_j\mathbf{u} = \omega^2\tilde{\mathbf{M}}_j\mathbf{u}$ CPU time (s)	0·65	0·66	0·65	0·63	0·66
Speed up time†	4·9	11·3	48	81·5	124·5

†The CPU time/flop count for solving the generalized eigenvalue problem for the five lowest eigenvalues and the corresponding eigenvectors is compared with the CPU time/flop count to solve a single subproblem for a single lowest eigenvalue and corresponding eigenvector. The speed up time/normalized flops is the ratio of these timings divided by five (since five such subproblems have to be solved to determine the five lowest eigenvalues and corresponding eigenvectors). It is to be noted that the time/flops for assembling the similarity transformation matrix T and the similarity transformation matrix multiplication is included in the computational effort for solving the subproblem.

execution and compared with the corresponding values for the standard method. The results of a few simulations are presented in Table 4. All the computations discussed in this section were carried out on an IBM RISC/6000 machine. The codes were written in MATLAB,‡ however, most of the significant computational work, such as assembling the stiffness matrix $\mathbf{K}$ and the orthogonal transformation matrices $\mathbf{T}_j$, was done using compiled Fortran MEX-files. The computation of the blocks in the identical block diagonalization of the mass matrix $\mathbf{M}$ and the stiffness matrix $\mathbf{K}$, i.e., the matrix multiplication associated with the similarity transformations $\tilde{\mathbf{K}}_j = \mathbf{T}_j^t\mathbf{K}\mathbf{T}_j$ and $\tilde{\mathbf{M}}_j = \mathbf{T}_j^t\mathbf{M}\mathbf{T}_j$, was carried out with the use of MATLAB's sparse multiplication capabilities.

The fully assembled symmetric stiffness matrix $\mathbf{K}$ and symmetric mass matrix $\mathbf{M}$ are stored in MATLAB's sparse storage format, i.e., only non-zero components and their indices are stored. The flop count and CPU timings for this step have not been shown in the comparison tables because this computation is required in both the standard and the group theoretic approach. The generalized eigenvalue problem is solved using MATLAB's EIGS function which finds a few eigenvalues and eigenvectors (we calculated the five

‡MATLAB is a registered trademark of the MathWorks, Inc.

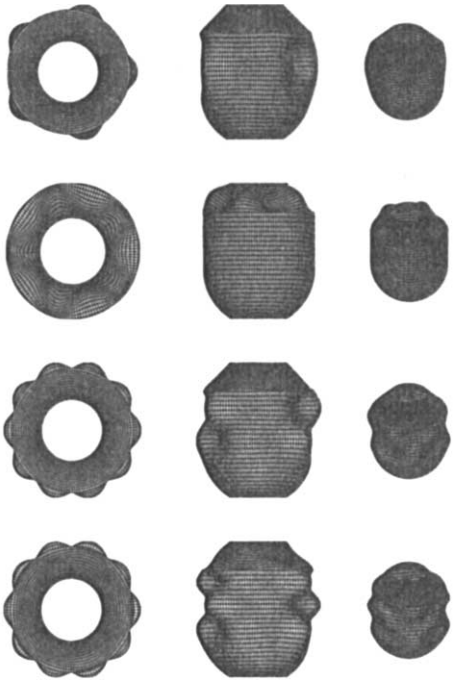

Figure 12. The mode shapes of a combination structure associated with the lower four frequencies in block 9.

lowest eigenvalues and associated eigenvectors) given a specified tolerance norm. The EIGS function utilizes the Fortran MEX-files of the ARPACK[§] routines which are Fortran programs for large size eigenvalue problems. The flop counts for five different problem sizes are shown in Table 4. The log-log plot in Figure 13 of the flop count against the problem size suggests that the computational cost of the given eigenvalue problem with sparse symmetric banded matrices is approximately $O(N^{1\cdot6})$. Here, N is the size of the stiffness matrix $\mathbf{K}$ and mass matrix $\mathbf{M}$. The subproblem size of each block in the block diagonalization is constant. The flop count of the subeigenvalue problem includes the cost of assembling the orthogonal transformation matrix $\mathbf{T}_j$ and the similarity transformation matrix multiplications $\tilde{\mathbf{K}}_j = \mathbf{T}_j^{\mathrm{t}}\mathbf{K}\mathbf{T}_j$ and $\tilde{\mathbf{M}}_j = \mathbf{T}_j^{\mathrm{t}}\mathbf{M}\mathbf{T}_j$. As discussed by Wohlever [5], there is a good deal of sparsity, repeated data and block diagonal structure in the orthogonal matrix $\mathbf{T}_j$. The matrices require relatively little memory when stored in the sparse format and lead to very efficient co-ordinate transformations. The normalized flop ratio is the ratio of the flop counts divided by five since five subproblems of similar size have to be solved to obtain the five lowest eigenvalues and eigenvectors of the given problem. However, it is to be noted that the group theoretic approach leads to independent subproblems which can be parallelly solved with availability of resources. As expected, the computational gain increases with increase in symmetry and varies from a factor of 5 for a problem with D_8 symmetry to around 200 for a problem with D_{64} symmetry (i.e., 64 elements along the circumference). The actual CPU timings are shown in Table 4. While the CPU time ratio is more modest compared to the flop count ratio, it is clear that the

[§]ARPACK routines available on http://www.caam.rice.edu/software/arpack/

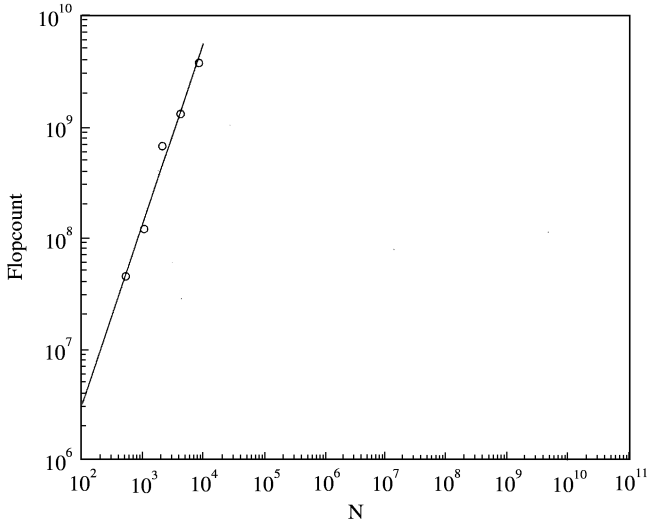

Figure 13. The log-log plot and the least square linear fit to determine exponential dependence of the computational effort of the generalized eigenvalue problem on the problem size. Here, N is the size of the square matrices **K** and **M**. The flop count is the number of floating point operations for the computation of the five lowest eigenvalues and the corresponding eigenvectors.

group theoretic approach offers significant computational savings in FEM analysis of problems with symmetry.

Wohlever [5] has discussed the computational savings in the solution of a linear system of equations $\mathbf{Ku} = \mathbf{f}$ in symmetry co-ordinates which arises in the static buckling problem of a cylinder. The presence of the minimum amount of symmetry, i.e., D_1 symmetry, leads to a decrease in CPU time by a factor of 2·5 as compared to the time required to solve the full problem in standard computational co-ordinates. A typical symmetry group for large problems could be D_{64}. This reduces CPU time by a factor of 100. For the problem of vibrations of shells with dihedral symmetry, we note that the representation of D_n on a mesh with m rings and n circumferential elements results in $4 + p + p$ blocks in the block diagonalization, where $p = (n - 2)/2$. Thus if $n = 100$ there are $4 + 49 + 49$ blocks where the first 49 blocks are identical to the next 49 blocks in eigenstructure. As per the discussions in section 4, only a few of these blocks (6 to 7 of the 49 blocks) need to be analyzed in the search for the first few natural frequencies (i.e., those with mode shapes of 0–6 or 7 circumferential waves). The subproblem sizes decrease by an order of 100 (D_{100} representation). Since eigenvalue computations are generally of $O(N^3)$, there are significant savings in computational effort.

6. CONCLUSIONS

In this paper, we have dealt with linear free vibrations of shells with dihedral symmetry. It is clear from the analyses and results discussed in this work that the group theoretic approach offers significant advantages for the linear free vibration analysis.

The group theoretic approach neatly separates out the analysis into physically meaningful subproblems. The vibrations of shells typically result in circumferential and longitudinal waves. The dihedral symmetry increases with the increase in the number of

circumferential waves. The same symmetry is reflected in the *isotropy subgroups* associated with the subproblems in the block diagonalization. *A priori* guesswork based on the geometry and the boundary conditions is not required. As a result, a large class of problems can be handled efficiently by a standard FEM code supplemented by group theoretic transformation routines. The class of practical problems of interest include shells with circumferential stiffeners and corrugated shells in addition to the examples discussed in this work. However, it should be ensured that the symmetry of the problem is imposed on the mesh.

The computational cost reduces dramatically due to the group theoretic approach because the original problem is split into independent subproblems in the block diagonalization. The block diagonalization leads to independent subproblems which retain the symmetry and band structure. The actual CPU timings and flop counts of numerical simulations shown in Table 4 suggest that these computational savings can be significant.

We also note that the group theoretic approach is useful for a linear transient response analysis. Linear transient response analysis under dynamic loads permit mode superposition techniques. The symmetry-adapted basis reduces the problem size just as in free vibration analysis. It is also useful in the identification of dominant modes of vibration to be used as the basis for the response of the structure.

The terms including the effect of shear deformation and rotary inertia are generally considered as complicating factors in free vibration analysis of shells. Neglecting shear deformation and rotary inertia is generally a very good approximation. The effects are significant only for short thick shells or when the number of circumferential and longitudinal waves are large, i.e., at higher frequencies. However, the terms involving the shear deformation and rotary inertia are included in the Simo element FEM shell equilibrium equations and are block diagonalized in the symmetry-adapted basis.

ACKNOWLEDGMENTS

This work has been supported by ISRO-IISc Space Technology Cell. The authors would like to thank Dr Chris Wohlever for his invaluable suggestions and for providing the kernel of his finite element routines.

REFERENCES

1. A. W. Leissa 1973 *Vibrations of Shells. NASA SP*-288 1973; U.S. Government Printing office.
2. W. Soedel 1993 *Vibrations of shells and plates*. New York: Marcel Dekker Publishers, second edition.
3. I. F. Niordson 1984 *International Journal of Solids and Structures* **20**, 669–687. Free vibrations of thin elastic spherical shells.
4. J. C. Wohlever and T. J. Healey 1995 *Computer Methods in Applied Mechanics and Engineering* **122**, 315–349. A group theoretic approach to the global bifurcation analysis of an axially compressed cylindrical shell.
5. J. C. Wohlever 1999 *Computer Methods in Applied Mechanics and Engineering* **170**, 373–406. Some computational aspects of a group theoretic finite element approach to the buckling and postbuckling analyses of plates and shells-of-revolution.
6. T. J. Healey and J. A. Treacy 1991 *International Journal for Numerical Methods in Engineering* **31**, 265–285. Exact block diagonalisation of large eigenvalue problems for structures with symmetry.
7. T. J. Healey 1988 *Computer Methods in Applied Mechanics and Engineering* **67**, 257–295. A group theoretic approach to computational bifurcation problems with symmetry.

8. K. Murota and K. Ikeda 1991 *SIAM Journal of Science and Statistical Computation* **12**, 273–297. Computational use of group theory in bifurcation analysis of symmetric structures.
9. J. C. Simo and D. D. Fox 1989 *Computer Methods in Applied Mechanics and Engineering* **72**, 267–304. On a stress resultant geometrically exact shell model. Part I: formulation and optimal parametrization.
10. J. C. Simo, D. D. Fox and M. S. Rifai 1989 *Computer Methods in Applied Mechanics and Engineering* **73**, 53–92. On a stress resultant geometrically exact shell model. Part II: the linear theory, computational aspects.
11. J. C. Simo, D. D. Fox and M. S. Rifai 1990 *Computer Methods in Applied Mechanics and Engineering* **79**, 21–70. On a stress resultant geometrically exact shell model. Part III: computational aspects of nonlinear theory.
12. J. C. Simo and D. D. Fox 1990 *Computer Methods in Applied Mechanics and Engineering* **81**, 91–126. On a stress resultant geometrically exact shell model. Part IV: variable thickness shells with through-the-thickness stretching.
13. J. L. Ericksen and C. Truesdell 1958 *Archives for Rational Mechanics and Analysis* **1**, 295–323. Exact theory of stress and strain in rods and shells.
14. A. W. Green and N. Laws 1966 *Proceedings of the Royal Society of London*, (O. D. Chwolson, editor) *Series A* **293**, 145–155. A general theory of rods.
15. A. E. Green and W. Zerna 1960 *Theoretical Elasticity*. Oxford: Clarendon Press, Oxford; second edition.
16. H. Cohen and C. N. DeSilva 1966 *Journal of Mathematical Physics* **7**, 960–966. Nonlinear theory of elastic directed surface.
17. P. M. Naghdi 1972 The theory of shells. in *Handbuch der Physic*: *Mechanics of Solids II* (C. Truesdell, editor) Berlin: Springer.
18. E. Cosserat and F. Cosserat 1909 Théorie des corps déformables. in *Traité de Physique*, 953–1173; second edition.
19. H. Ahmed, B. M. Irons and O. C. Zienkiewicz 1970 *International Journal for Numerical Methods in Engineering* **2**, 419–451. Analysis of thick and thin shell structures by curved finite elements.
20. A. E. Green, P. M. Naghdi and M. L. Wenner 1971 *Proceedings of the Cambridge Philosophical Society* **69**, 227–254. Linear theory of Cosserat surface and elastic plates of variable thickness.
21. T. H. H. Pian and K. Sumihara 1984 *International Journal for Numerical Methods in Engineering* **20**, 1685–1695. Rational approach for assumed stress finite elements.
22. J. C. Simo and T. J. R. Hughes *Journal of Applied Mechanics* **53**, 51–54. On the variational foundations of assumed strain methods.
23. J. C. Simo, M. S. Rifai and D. D. Fox 1992 *International Journal for Numerical Methods in Engineering* **34**, 117–164. On a stress resultant geometrically exact shell model. Part *VI*: conserving algorithms for nonlinear dynamics.
24. H. Kraus 1967 *Thin Elastic Shells*. New York: Wiley.
25. R. N. Arnold and G. B. Warburton 1949 *Proceedings of the Royal Society London*, *Series A* **197**, 238–256. Flexural vibrations of the walls of thin cylindrical shells having freely supported ends.
26. E. I. Grigolyuk 1956 *Izvestiya Akademii Nauk SSR*, *O.T.D* **6**, 35–44. NASA TT F-25. Small oscillations of thin elastic shells.
27 D. H. Platus 1965 *Conical Shell Vibrations*. NASA TN D-2767.
28 W. Miller 1972 *Symmetry*, *Groups and their Applications*. New York: Academic Press.
29 A. Fassler and E. Stiefel 1992 *Group Theoretical Methods and their Applications*. Boston: Birkhauser.

APPENDIX A: THE GROUP THEORETIC APPROACH TO THE SOLUTION OF THE GENERALIZED LINEAR EIGENVALUE PROBLEM

The central ideas and theorems of group theory leading to equation (2) are outlined here. The details are given in many excellent texts, cf. books by Miller [28] or by Fässler and Stiefel [29]. The explicit formulae and the algorithm for the construction of the orthogonal transformation matrix, **T**, and the analysis of the associated computational complexity is discussed by Murota and Ikeda [8]. These formulae are applicable for trusses with dihedral symmetry. The modification of these formulae for the analysis of the discretized finite element shells equations is discussed by Wohlever [5]. The discussion on the identical block diagonalization of the stiffness matrix **K** and the mass matrix **M** (see Appendix A.3) is reproduced from the paper by Healey and Treacy [6].

A.1. SOME BASIC RESULTS FROM GROUP THEORY

Let G be a finite group, whose order is denoted by $|G|$ and V a finite-dimensional vector space. Let $GL(V)$ be the group of all non-singular linear transformations of V onto itself.

Definition 1. A representation of G on V is a homomorphism $H : G \to GL(V)$, i.e.,

$$H(gh) = H(g)H(h), \quad \forall g, h \in G. \tag{A.1}$$

V is the representation space and $n = dim(V)$, the dimension of the group representation. The linear transformations $H(g)$ can be associated with the $n \times n$ non-singular matrices on fixing a basis for V.

Definition 2. Two matrix group representations of G, H_1 and H_2 are said to be equivalent if there exists a non-singular matrix B such that

$$H_1(g) = B^{-1}H_2(g)B, \quad \forall g \in G. \tag{A.2}$$

A subspace W of V is said to be G invariant if $H(g)w \in W \ \forall w \in W$ and $\forall g \in G$.

Definition 3. A representation, H of G on V, is said to be *irreducible* if there exists no non-trivial subspace W (i.e., W can only be $\{0\}$ or V).

Definition 4. A representation, H of G on V, is said to be *completely reducible* if every invariant subspace $W \subset V$ has an invariant complement U. This implies $V = W \oplus U$.

In such a case, we say that the representation H reduces to irreducible representations $H_1, \ldots, H_N$ on vector spaces $V_1, \ldots, V_N$, respectively, such that $V = V_1 \oplus \cdots \oplus V_N$. In order to express the reduction of the representation H into the representations $H_1, \ldots, H_N$, we write $H = H_1 \oplus \cdots \oplus H_N$.

Theorem 5. *A finite group G of order $|G|$ has only a finite number of inequivalent irreducible representations H_j. We denote the dimension of H_j by n_j.*

The important groups for our applications are the dihedral groups. The rotational and reflection symmetries of a regular polygon of n sides form the dihedral group D_n of order $2n$. $D_n = \{1, r, \ldots, r^{n-1}; s, sr, \ldots, sr^{n-1}\}$, where $r^n = s^2 = (sr)^2 = 1$. The group elements r and s are the generators of the group.

There are N non-equivalent irreducible representations which can be indexed as

$$R(D_n) = \{(1,j)\,|\,j = 1,2,3,4\} \cup \{(2,j)\,|\,j = 1,\ldots,(n-2)/2\} \text{ for } n \text{ even},$$
$$R(D_n) = \{(1,j)\,|\,j = 1,2\} \cup \{(2,j)\,|\,j = 1,\ldots,(n-1)/2\} \text{ for } n \text{ odd},$$

where the first component d of the index $N = (d,j)$ indicates the dimension of the representation.

The one-dimensional irreducible representations $H^{(1,j)}$ of D_n are given by

$$H^{(1,1)}(r) = 1, \qquad H^{(1,1)}(s) = 1,$$
$$H^{(1,2)}(r) = 1, \qquad H^{(1,2)}(s) = -1,$$
$$H^{(1,3)}(r) = -1, \qquad H^{(1,3)}(s) = 1,$$
$$H^{(1,4)}(r) = -1, \qquad H^{(1,4)}(s) = -1.$$

The two-dimensional irreducible representations $H^{(2,j)}$ of D_n are given by

$$H^{(2,j)}(r) = R^j, \qquad H^{(2,j)}(s) = S,$$

where

$$R = \begin{pmatrix} \cos(2\pi/n) & -\sin(2\pi/n) \\ \sin(2\pi/n) & \cos(2\pi/n) \end{pmatrix}, \qquad S = \begin{pmatrix} 1 & 0 \\ 0 & -1 \end{pmatrix}.$$

We note that the representations are by 1×1 and 2×2 orthogonal matrices.

Theorem 6. *Every orthogonal representation H is completely reducible.*

Thus, any representation H of a group G on an n-dimensional vector space V by orthogonal matrices is completely reducible and is given by

$$H = c_1 H_1 \oplus c_2 H_2 \oplus \cdots \oplus c_n H_n, \tag{A.3}$$

where the H_j are irreducible and mutually inequivalent representations of G. The numbers $c_j \in \{1,2,3,\ldots\}$ indicate the multiplicity. Let n_j be the dimension of H_j. Accordingly, the representation vector space V of H decomposes into

$$V = V_1 \oplus V_2 \oplus \cdots \oplus V_n. \tag{A.4}$$

This is called the isotypic decomposition of V and is uniquely determined as are the multiplicities c_j. However, the decomposition of an isotypic component V_j into c_j number of n_j-dimensional irreducible subspaces is, in general, not unique. A particular choice is useful for applications. This is the substance of the fundamental theorem for group theoretic applications.

A.2. THE FUNDAMENTAL THEOREM

Definition 7. Let L be a linear operator, mapping an *n-dimensional* vector space V into itself. L has the symmetry of the group representation H of the group G if it commutes with every representing matrix, i.e.,

$$LH(g) = H(g)L \quad \forall g \in G.$$

Theorem 8. *Let $H : g \to H(g)$ be an n-dimensional completely reducible representation of a group G. Let the complete reduction be given by*

$$H = c_1 H_1 \oplus c_2 H_2 \oplus \cdots \oplus c_n H_n, \tag{A.5}$$

where H_j are the irreducible and mutually inequivalent representations of G. The numbers $c_j \in \{1, 2, 3, \ldots\}$ indicate the multiplicity and n_j the dimension of H_j. Then there exists a basis of the isotypic subspaces V_j in which a symmetric linear operator L decomposes into a direct sum of

n_1 *identical square matrices* L_1 *of length* c_1

n_2 *identical square matrices* L_2 *of length* c_2

$\vdots$

n_N *identical square matrices* L_N *of length* c_N.

This is the block diagonalization of the linear operator L.

A.3. THE IDENTICAL BLOCK DIAGONALIZATION OF THE STIFFNESS MATRIX **K** AND MASS MATRIX **M**

Let the total energy of a symmetric linear structure under free vibrations be E. Thus, E is the sum of the kinetic and potential energies.

$$E(\dot{\mathbf{u}}, \mathbf{u}) = \tfrac{1}{2}(\dot{\mathbf{u}}^{\mathrm{t}}\mathbf{M}\dot{\mathbf{u}} + \mathbf{u}^{\mathrm{t}}\mathbf{K}\mathbf{u}). \tag{A.6}$$

Here, $\mathbf{u}$ and $\dot{\mathbf{u}}$ are displacement and velocity vectors. Symmetric structures enjoy special properties. Some of these are characterized mathematically in terms of transformations upon the energy. The orthogonal group representing matrices $H(g)$ $g \in G$ are linear transformations of the displacement vector field that leave the total energy invariant, i.e.,

$$E(H(g)\dot{\mathbf{u}}, H(g)\mathbf{u}) = E(\dot{\mathbf{u}}, \mathbf{u}), \quad \forall g \in G. \tag{A.7}$$

More generally, equation (A.6) represents the total energy of an n-d.o.f. system, for which the symmetry is characterized by some group, say G. We note that equation (A.7) is valid for all possible displacements and velocities. On differentiating both sides of equation (A.7) with respect to $\mathbf{u}$ and $\dot{\mathbf{u}}$, respectively, we deduce that

$$\mathbf{M}H(g) = H(g)\mathbf{M} \quad \text{and} \quad \mathbf{K}H(g) = H(g)\mathbf{K}, \quad \text{for } \forall g \in G. \tag{A.8}$$

Thus, $\mathbf{M}$ and $\mathbf{K}$ each commute with the entire family of transformations of the group representation H. Therefore, the fundamental theorem asserts that there is a symmetry-adapted basis of the vector space V in which symmetric linear operators $\mathbf{M}$ and $\mathbf{K}$ are block diagonalized.

A.4. SIGNIFICANCE OF THE BLOCK DIAGONALIZATION

It is clear from the fundamental theorem that

(1) A problem defined by symmetric operators is split up into lower dimensional independent subproblems.

(2) One can determine *a priori* the size of the lower dimensional matrices.

(3) One can determine *a priori* the number of subproblems which are identical in nature.

Moreover, each subspace V_j of the isotypic decomposition reflects part of the symmetry of the original system. This leads to physical insights unique to the group theoretic approach.

Definition 9. A subgroup $SG' \subseteq G$ is an isotropy subgroup associated with a vector space V if the orthogonal representation matrices of SG', $H(g')$ for $g' \in SG'$, leave every vector in the vector space invariant, i.e., $H(g')\mathbf{u} = \mathbf{u}$, $\forall \mathbf{u} \in V$, and $\forall g' \in SG'$.

The isotropy subgroups associated with the dihedral group are discussed by Mutota and Ikeda [8]. The subspace V_1 is typically designated as the G-invariant subspace which implies that the elements of V_1 reflect the symmetry of the complete group G. For example, V_1 might represent the set of all axisymmetric solutions in a problem with circular symmetry. The *isotropy subgroups* $SG'(V_j)$ associated with the subspace V_j are as follows:

$$SG'(V_1) = D_n, \qquad SG'(V_2) = C_n, \qquad SG'(V_3) = SG'(V_4) = D_{n/2}, \tag{A.9}$$

$$SG'(V_{4+j}) = D_{gcd(n,j)}, \quad j = 1, \ldots \frac{n-1}{2}. \tag{A.10}$$

The operator $gcd(n,j)$ is the greatest common divisor of n and j. Thus each of the blocks in the block diagonalization of the stiffness matrix $\mathbf{K}$ and mass matrix $\mathbf{M}$ (equation (A.10)) group together all the vibration modes which possess the symmetry of the associated *isotropy subgroup*.